



# Graphene nanoplatelet/cellulose acetate film with enhanced antistatic, thermal dissipative and mechanical properties for packaging

Zijun Gao · Yao Li · Pei Huang · Rui Zou ·  
Yuanqing Li · Shaoyun Fu

Received: 16 December 2022 / Accepted: 18 March 2023 / Published online: 1 April 2023  
© The Author(s), under exclusive licence to Springer Nature B.V. 2023

**Abstract** With the increased concern over environment protection, cellulose acetate (CA) has drawn great interests as an alternative for packaging material due to its biodegradability and abundant resources; whereas, the poor antistatic property and thermal conductivity restrict its application in packaging. In this work, we proposed a simple but effective strategy to produce high performance graphene nanoplatelet (GNP)/CA composite films via the consecutive homogenization and solvent casting processes.

Relying on the spontaneous absorption of CA during homogenization, the GNP/CA produced shows an excellent dispersibility in the N,N-Dimethylformamide (DMF) solution and many fewer structural defects compared with GNPs alone. As a result, the composite films obtained exhibit simultaneously and significantly enhanced antistatic, heat dissipative and mechanical properties compared with CA. Specifically, the GNP/CA composite with the optimal formula has promising overall performances (namely, surface resistivity of  $3.33 \times 10^7 \Omega/\text{sq}$ , in-plane thermal conductivity of  $5.359 \text{ W(m} \cdot \text{K)}$ , out-of-plane thermal conductivity of  $0.785 \text{ W(m} \cdot \text{K)}$ , and tensile strength of  $37.1 \text{ MPa}$ ). Featured by its promising overall properties, simple production processes and biodegradability, the as-prepared GNP/CA composite film shows a great potential for application in packaging.

**Supplementary Information** The online version contains supplementary material available at <https://doi.org/10.1007/s10570-023-05155-2>.

Z. Gao · Y. Li · P. Huang (✉) · Y. Li · S. Fu (✉)  
College of Aerospace Engineering, Chongqing University,  
Chongqing 400044, China  
e-mail: p.huang@cqu.edu.cn

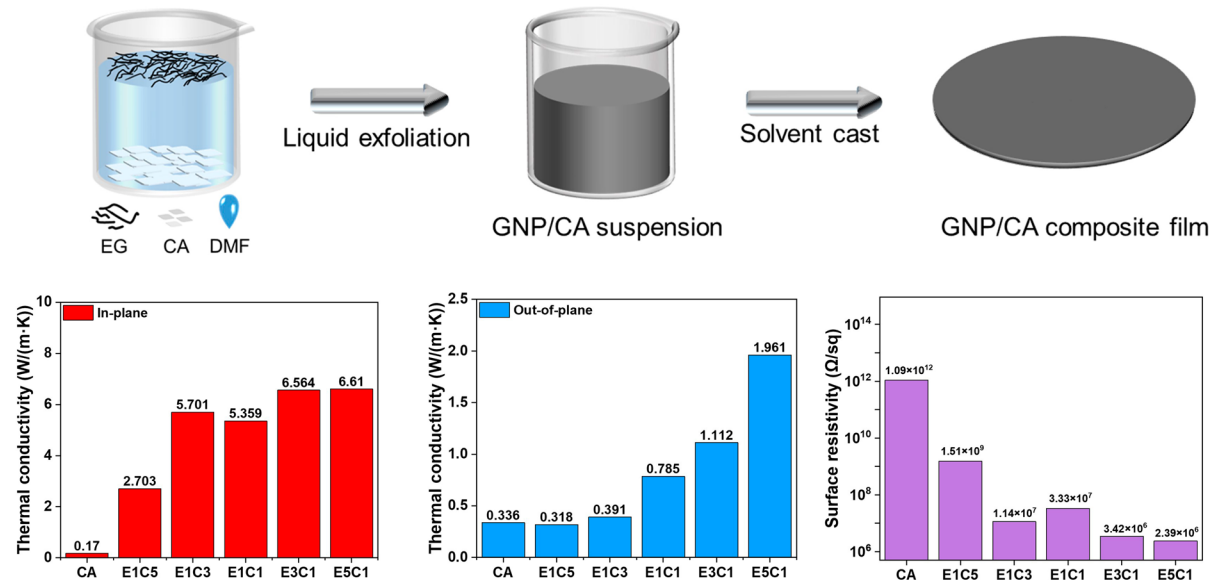
S. Fu  
e-mail: syfu@cqu.edu.cn

Z. Gao · Y. Li · P. Huang · Y. Li · S. Fu  
State Key Laboratory of Power Transmission Equipment  
and System Security and New Technology, Chongqing  
University, Chongqing 400044, China

R. Zou  
State Key Laboratory of Reliability and Intelligence  
Electrical Equipment, Hebei University of Technology,  
Tianjin 300130, China

R. Zou  
School of Mechanical Engineering, Hebei University  
of Technology, Tianjin 300401, China

## Graphical Abstract



**Keywords** Graphene nanoplatelet · Cellulose acetate · Composite · Antistatic

## Introduction

The wide spread of Covid-19 pandemic has boosted the rapid development of online purchasing, thus leading to the increased consumption on packaging materials in the last 3 years. Currently, the mainstream material used for packaging is non-degradable plastics, such as polyethylene (PE), polypropylene (PP), polyvinyl chloride (PVC), polyethylene terephthalate (PET) and other petroleum-based synthetic plastics, which brings about serious environmental contamination (Lazarevic et al. 2010; Mangaraj et al. 2018; Shaikh et al. 2021; Wu et al. 2021). Although numerous academic research efforts have been paid to biodegradable polymers (Dong et al. 2015; Nagarajan et al. 2016; Samantaray et al. 2020), few bio-based/biodegradable polymers have been successfully commercialized for packaging so far due to high cost and complicated production processes. Featured by biodegradability and natural abundance, cellulose acetate

(CA) has been widely used in industry and biomedicine (Buchanan et al. 1993; Kaiser et al. 2017; Konwarh et al. 2013; Seddiqi et al. 2021; Taepaiboon et al. 2007; van Someren et al. 1974; Zugenmaier. 2004). Additional advantages, such as excellent thermal stability, low permissibility to methanol and enriched functional groups, etc., recognize CA as an ideal alternative for packaging material (Araujo et al. 2020; Claro et al. 2016; Gemili et al. 2009; Muhmed et al. 2020; Rajeswari et al. 2020; Wondraczek et al. 2013). However, CA has a poor antistatic property and thermal conductivity, of which the former causes the accumulation of static electricity and thereafter severe problems (e.g. attracting dust, intertwisting and electric shocks), and the latter delays the dissipation of heat generated by high-voltage electronics, li-ion battery and other devices inside, thus hindering its application in the field of packaging (Basu et al. 2016; Iradukunda et al. 2020; Tan et al. 2020). In this regard, it is highly desirable to develop a CA-based packaging material with enhanced antistatic and heat dissipative properties.

To improve the antistatic and heat dissipative properties of polymers, the most facile strategy is to introduce electrically and thermally conductive fillers,

such as carbon, metal and metal oxide materials (de Moraes et al. 2015; El-Din et al. 2015; Elmaghraby et al. 2022; Liu et al. 2013; Rajeswari et al. 2017). In comparison, graphene, a two-dimensional (2D) monolayer of carbon atoms, is taken to be an excellent candidate to improve the antistatic and thermal properties of polymers owing to its superior electron mobility ( $2.5 \times 10^5 \text{ cm}^2/(\text{V} \cdot \text{s})$ ) and thermal conductivity ( $5300 \text{ W}/(\text{m} \cdot \text{K})$ ) (Balandin et al. 2008; Novoselov et al. 2012). Meanwhile, the ultra-high mechanical properties of graphene could spontaneously endow the composite improved mechanical properties. However, the dispersion of graphene in polymer matrix remains a big challenge because of its high aspect ratio and surface energy (Biswas & Drzal. 2009). To overcome this difficulty, one may use surfactant to assist the dispersion of graphene, but it would sacrifice the electrical and mechanical properties of the composite produced (Tkalya et al. 2012). By contrast, introducing the targeted polymer during graphene exfoliation enables the well-dispersion of graphene and thereafter improves the properties of the composite produced, hence being distinguished as one of the most promising approaches to fabricate graphene-based composites. For instance, the use of melt-blending to assist the dispersion of graphene in polypropylene provides the obtained composite an increase of 43% in Young's modulus (Lee et al. 2020). The liquid exfoliation of graphite in the presence of sodium carboxymethyl cellulose gives a better dispersion of graphene as well as a higher capacity of the composite produced than that of the commercial graphite in Li-ion (Naboka et al. 2016). Since a similar structure to cellulose or cellulose derivatives would provide CA a good compatibility with graphene, it is plausibly expected to improve the dispersion of graphene nanoplatelets (GNPs) and hence the antistatic, heat dissipative and mechanical property of CA composite via the simultaneous homogenization of CA and expanded graphite (EG).

Herein, the liquid exfoliation of EG in CA solution and the subsequent solvent casting are adopted to produce GNP/CA composite films. Relying on the excellent compatibility between GNPs and CA, the spontaneous absorption of CA provides GNPs an excellent dispersibility in DMF and fewer structural defects as well. As a result, the GNP/CA composite film obtained has a greatly decreased surface resistivity and significantly increased thermal

conductivity at both the in-plane and out-of-plane directions, therefore allowing the rapid dissipation of static electricity and heat. Moreover, the GNP/CA composite film produced shows an improved mechanical strength. In view of the improved antistatic, heat dissipative and mechanical properties as well as simple production, the GNP/CA composite film shows a great promise in packaging.

## Experimental section

### Materials

EG (99.9%) was received from Qingdao Hengrunda Graphite Co., Ltd. Ethanol (99.5%) and DMF (99.7%) were supplied by Chengdu Kelong Chemical Reagents Co., Ltd. CA with acetyl content of 55% was purchased from Shanghai Zhanyun Chemical Co., Ltd. All chemical reagents were used as received.

### Fabrication of GNP/CA composite film

Firstly, 3 g EG was added into 600 mL DMF solution of CA, and then subjected to a homogenizer (JRJ300, Shanghai Hu Xi Industrial Co., Ltd.) at 6000 rpm for 90 min. Secondly, the supernatant of GNP/CA dispersion obtained was left to stand for 24 h. Followed by oven-dry at 90 °C, the GNP/CA composite film was obtained. For convenience, the GNP/CA composite film was labeled as ExCy, where x and y are the initial weight ratio of EG and CA in their mixture, respectively. When no CA is added during the homogenization process, the product obtained was named as GNPs.

### Characterizations

Morphologies of EG, GNPs, CA and GNP/CA composite films were characterized by a scanning electron microscope (SEM, Thermal Scientific, Quattro S, US) operated at 20 kV. Prior to be sputtered with gold, the SEM samples for GNPs were produced by depositing a droplet of diluted DMF suspension of pure GNPs or GNP/CA onto the Si wafer while EG, CA film and GNP/CA composite films were directly attached to the stage by the conductive adhesive. Thermal gravimetric analysis (TGA) was performed on a NETZSCH TG209F3 Tarsus under air atmosphere

at the heating rate of 10 °C/min from 100 to 950 °C. X-ray photoelectron spectroscopy (XPS) characterizations of EG and GNP powders were recorded by an ESCALAB 250Xi (Thermo Electron). Raman spectra of GNP/CA composite films were obtained by a LabRAM HR Evolution with a 532 nm laser source. The atomic force microscope (AFM) images of GNPs and GNP/CA were taken by a Multimode 8 (cantilever data: T: 650 nm, L: 115 μm, W: 25 μm,  $f_0$ : 70 Hz, k: 0.4 N/m) via the tapping mode. The samples for AFM were prepared by depositing a droplet of diluted DMF suspension of GNPs or GNP/CA onto the Si wafer. The tensile strength of the composite films was measured by a Shimadzu EZ-LX at a displacement rate of 1 mm/min. The specimens were cut into a rectangular shape with 5 mm in width and 20 mm in length, and 10 specimens were tested for each composition. Sheet resistance was measured by a Keithley 6517B Electrometer/High Resistance Meter following the standard of ASTM D257. The in-plane and out-of-plane thermal diffusivity was measured by a LFA-467 NanoFlash via flash diffusivity technique in horizontal and vertical conduction mode, respectively. The specific heat capacity was obtained by a differential scanning calorimeter (Netzsch STA449 F3) at 25 °C. Therefore, the thermal conductivity ( $K$ ) of the composite was calculated by using the following equation.

$$K = \alpha \cdot \rho \cdot C_p \quad (1)$$

where  $\alpha$ ,  $\rho$  and  $C_p$  represent the thermal diffusivity, density and specific heat capacity of the composite, respectively.

## Results and discussions

### Fabrication of GNP/CA composite film

As shown in Fig. 1a, the GNP/CA composite film was produced by the consecutive liquid exfoliation and solvent casting processes. In brief, EG and CA were simultaneously homogenized in DMF at 6000 rpm for 90 min. Afterwards, the suspension obtained was left to stand for 24 h. Finally, the supernatant was collected and oven-dried at 90 °C for 4 h, thus obtaining a GNP/CA composite film (Fig. 1b). Although both the GNPs and GNP/CA produced

show similar morphologies (ca. 4 nm in thickness and several microns in lateral dimension, see Fig. 1c–g and S1), their dispersibility in DMF exhibit a great difference. As shown in Fig. 1h, pure GNPs gradually precipitate, and the supernatant transforms to transparent solution after 24 h. In comparison, the GNP/CA produced shows a much higher stability in DMF, as no detectable sediment was formed after 24 & 48 h and the occurrence of Tyndall effect was observed when a laser passes through (Figs. 1i and S2).

In addition to the improved dispersibility, the GNPs in GNP/CA system exhibit much fewer structural defects. As shown in Fig. 2a, all GNP/CA composites present characteristic D-peak ( $1350 \text{ cm}^{-1}$ ) and G-peak ( $1580 \text{ cm}^{-1}$ ), which are assigned to the disorder-induced  $A_{1g}$  zone-phonon and crystalline graphite arising from the zone-center  $E_{2g}$  mode, respectively. The  $I_D/I_G$  value is shifted from 0.06 for EG to 0.26 for GNPs, suggesting the increased number of structural defect due to the high-speed homogenization and presence of oxygen in the solvent. However, the GNPs in E5C1 have a decreased  $I_D/I_G$  value of 0.23. Further increasing the CA content leads to the continuous decrease of  $I_D/I_G$ . To be specific, E1C5 has an  $I_D/I_G$  value of 0.1, close to that of EG. Similar results were obtained from XPS analysis. As presented in Table S1 and Fig. 2b, the C/O ratio of EG is decreased from 26.8 to 10.8 after mechanical exfoliation. Despite CA has a low C/O ratio of 1.6, the GNPs (labeled as G-C) obtained from 3 cycles of centrifugation of GNP/CA at 10,000 rpm for 20 min have a C/O ratio of 14.2, higher than that of pure GNPs, suggesting less structural deformation occurs to GNPs in the presence of CA. The reason for the improved dispersibility and structural integrity is that the spontaneous absorption of CA via CH- $\pi$  interaction endows the GNPs an steric hindrance to DMF as well as oxygen (Alqus et al. 2015; Han et al. 2019). The surface existence of CA was confirmed by FT-IR analysis. As shown in Fig. 2c, the peak at  $1750 \text{ cm}^{-1}$ , assigned to C=O vibration in acetyl group, is observed in CA and G-C, but not in EG and GNPs (Fei et al. 2017; Zhang et al. 2011). Since free CA was removed by centrifugation, the CA detected by FT-IR is located on the surfaces of GNPs via physical absorption.

Considering most of the original EG fails to be exfoliated, the thermal gravimetric analysis of GNP/CA composites was thus performed to reveal their GNP content. As shown in Fig. 3a, CA is completely

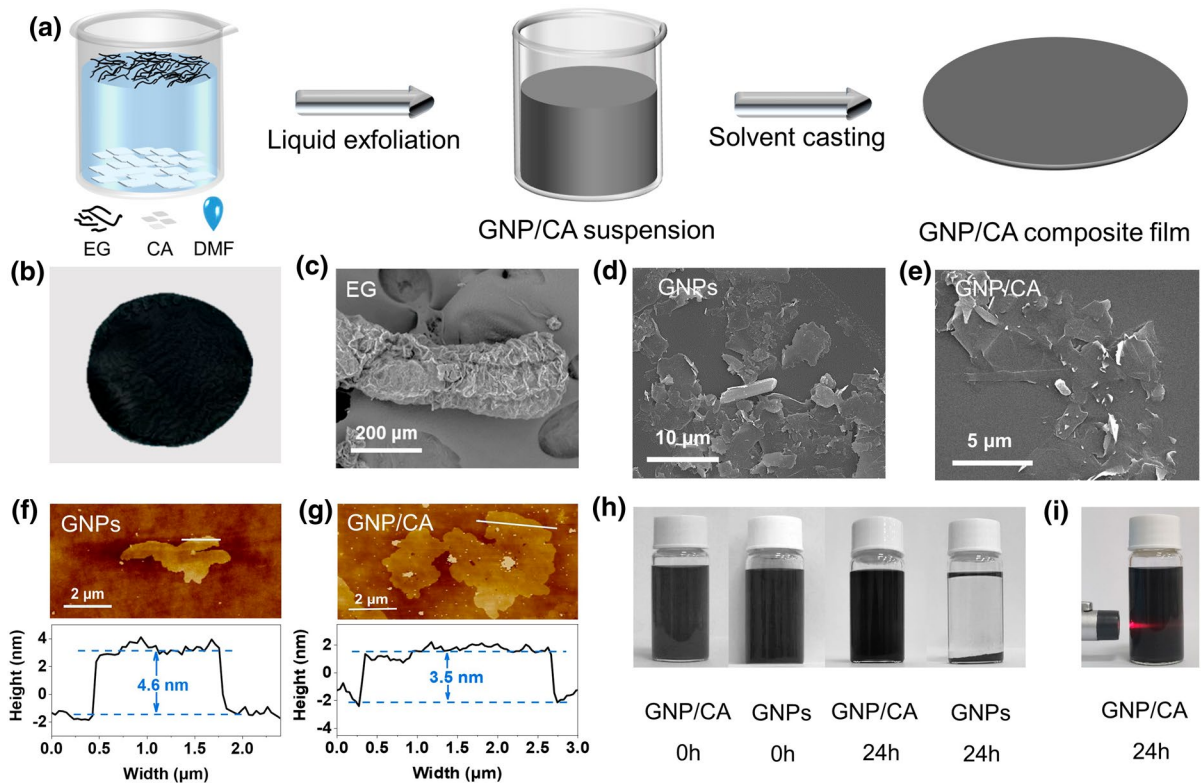


**Fig. 1** (a) Schematics for the production of GNP/CA composite film; (b) optical image of the GNP/CA composite film; (c–e) SEM images of (c) EG, (d) GNPs and (e) GNP/CA; (f–g) AFM images of (f) GNPs and (g) GNP/CA; (h) optical images

of GNP and GNP/CA suspension after standing for various times; (i) optical image of the DMF suspension of GNP/CA when a laser passes through

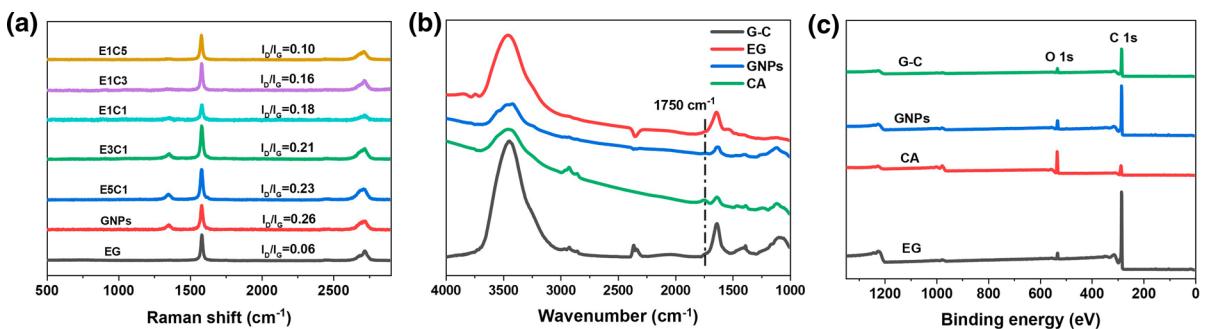


**Fig. 2** (a) Raman spectra of EG, GNPs and GNP/CA composite films, (b) FTIR and (c) XPS spectra of EG, CA, GNPs and G-C

decomposed at  $550\text{ }^\circ\text{C}$  where GNPs have negligible weight loss under air atmosphere. Therefore, the weight percentage at  $550\text{ }^\circ\text{C}$  is determined as the GNP content of the GNP/CA composite. It is worthy to mention that the decomposition temperature

of pure GNPs is higher than that of GNPs in GNP/CA composites. This is due to the fact that, with the increase of temperature, the gradual decomposition of CA initially transforms the GNP/CA composite to a porous GNPs sponge, which has a much larger

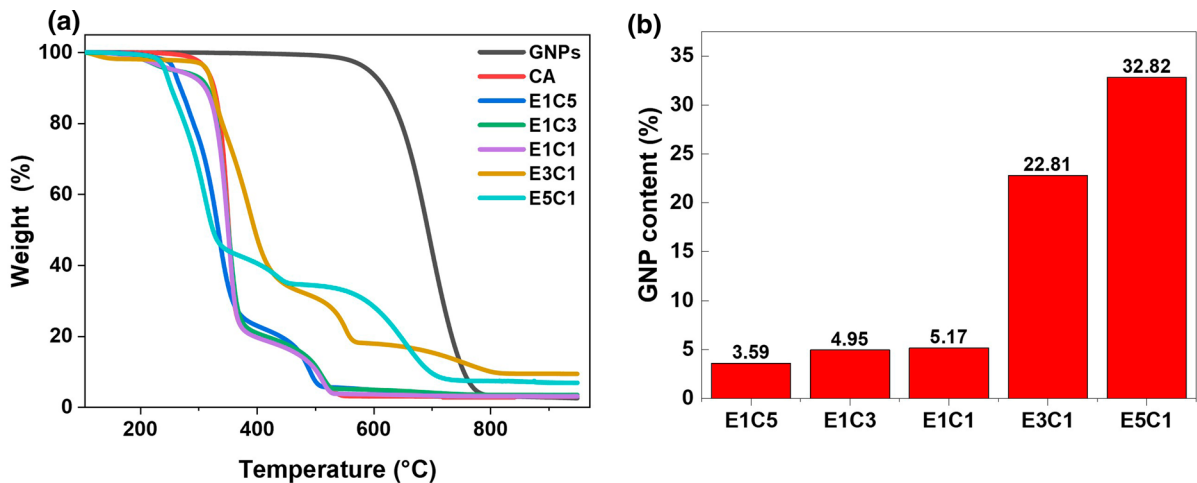


**Fig. 3** (a) TGA curves of GNPs, CA and GNP/CA composites under air atmosphere; (b) GNP content of GNP/CA composites

specific surface area and therefore higher reactivity than pure GNPs (Farivar et al. 2021; Jiang et al. 2000). For the case of EG/CA ratio of 1:5, the composite produced has a GNP content of 3.59%, which is much lower than the original EG content. Further rising the EG/CA ratio to 1:1 slightly increases the GNP content to 5.17%. Notably, the GNP content sharply increases to 22.81% and 32.82% as the EG/CA ratio increases to 3:1 and 5:1. Due to the fact of no free-standing composite film can be obtained when EG/CA ratio is higher than 5:1, a maximum EG/CA ratio of 5:1 was hence used in the following studies.

#### Antistatic property of GNP/CA composite film

According to ASTM D257-78, the surface resistivity of antistatic materials needs to fall in the range of  $1.0 \times 10^5$  to  $1.0 \times 10^{12}$   $\Omega/\text{sq}$  (Groop et al. 2003; Ho Shin et al. 2006). Due to the high surface resistivity of  $1.09 \times 10^{12}$   $\Omega/\text{sq}$  (Fig. 4), CA is unable to dissipate static electricity spontaneously. In comparison, the GNP/CA composites have a significantly decreased surface resistivity. For instance, E1C5 has a surface resistivity of  $1.51 \times 10^9$   $\Omega/\text{sq}$ , comparable to that of the composites with similar GNP loading (Table S2). However, increasing the EG/CA ratio from 1:3 to 1:1 leads to a slight increase of surface resistivity from  $1.14 \times 10^7$  to  $3.33 \times 10^7$   $\Omega/\text{sq}$ . The reason for this is, although E1C1 has a slightly higher GNP content than E1C3 (Fig. 3b), the cracks and holes observed on

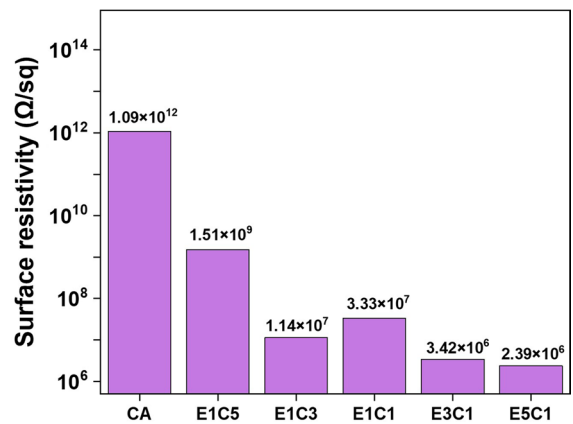


**Fig. 4** Surface resistivity of CA and GNP/CA composite films

E1C1 surface (while no observable cracks and holes on E1C3 surface, see Fig. S3) would have a negative influence on static dissipation by disrupting the dissipative pathway (Wang et al. 2018). Owing to the similar element composition between CA and GNPs, EDS fails to evaluate the distribution of GNPs on the surface of composite (see Fig. S3). The surface resistivity of composite is further decreased as the EG/CA ratio increases up to 3:1 and 5:1 owing to the sharply increased GNP content. But the ratio of surface resistivity decrease is decreased because of the increased surface defects. Nevertheless, all the GNP/CA composites fall within the range of antistatic materials. By contrast, other composites of such a high graphene or GNP content have a much lower resistivity (Wang

et al. 2017). This discrepancy might be due to the fact that the surface absorption of CA leads to the electrical insulation between neighboring GNPs (Morishita & Matsushita. 2021; Vu et al. 2018).

#### Thermal conductivity of GNP/CA composite film

Figure 5a shows the thermal conductivity ( $\parallel$ ) of GNP/CA composite films in the in-plane direction. Pure CA film has a poor thermal conductivity ( $\parallel$ ) of 0.170 W/(m · K), consistent with the previous report (Suthabanditpong et al. 2019). Notably, the thermal conductivity ( $\parallel$ ) of the GNP/CA composites is significantly increased. For the case of E1C5 and E1C3, their corresponding thermal conductivity ( $\parallel$ ) is 2.703 and 5.701 W/(m · K), achieving an increase of 1490% and 3253%, respectively. Increasing the EG/CA ratio up to 5:1 gives rise to a slight increase of thermal conductivity ( $\parallel$ ) up to 6.61 W/(m · K), agreeing well with the tendency of anti-static property. Regarding the out-of-plane direction, the thermal conductivity ( $\perp$ ) of composite maintains at a lower level due to the low thermal conductivity ( $\sim$ 10–20 W/(m · K)) of graphene in the out-of-plane direction (Balandin. 2011). It should be noted that the thermal conductivity of CA in the out-of-plane direction differs from that in the in-plane direction because of the different characterization methods applied. Even though, the results indicate the thermal conductivity ( $\perp$ ) of the GNP/CA composites is greatly improved. As shown in Fig. 5b, E1C5 has a

thermal conductivity ( $\perp$ ) of 0.318 W/(m · K), close to that of pure CA (0.336 W/(m · K)). The increment of EG/CA ratio to 1:3 gives rise to the steady increase of thermal conductivity to 0.391 W/(m · K). As the EG/CA ratio increases to 1:1, 3:1 and further to 5:1, the thermal conductivity ( $\perp$ ) is sharply increased to 0.785, 1.112 and further to 1.961 W/(m · K), achieving an increase of 133%, 231% and 483%, respectively. Such a high thermal conductivity in both the in-plane and out-of-plane direction enables the GNP/CA composite film dissipate heat rapidly, thus providing protection to the item packed inside.

#### Tensile strength of GNP/CA composite film

Besides the antistatic and heat dissipative properties, the tensile strength of composite is also improved.

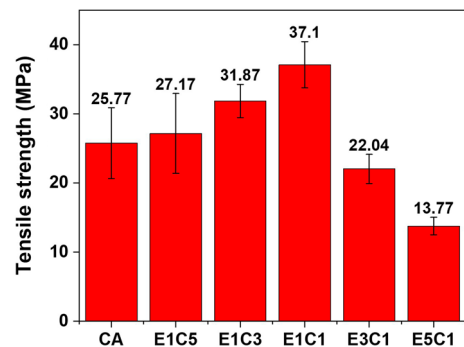


Fig. 6 Tensile strength of CA and GNP/CA composite films

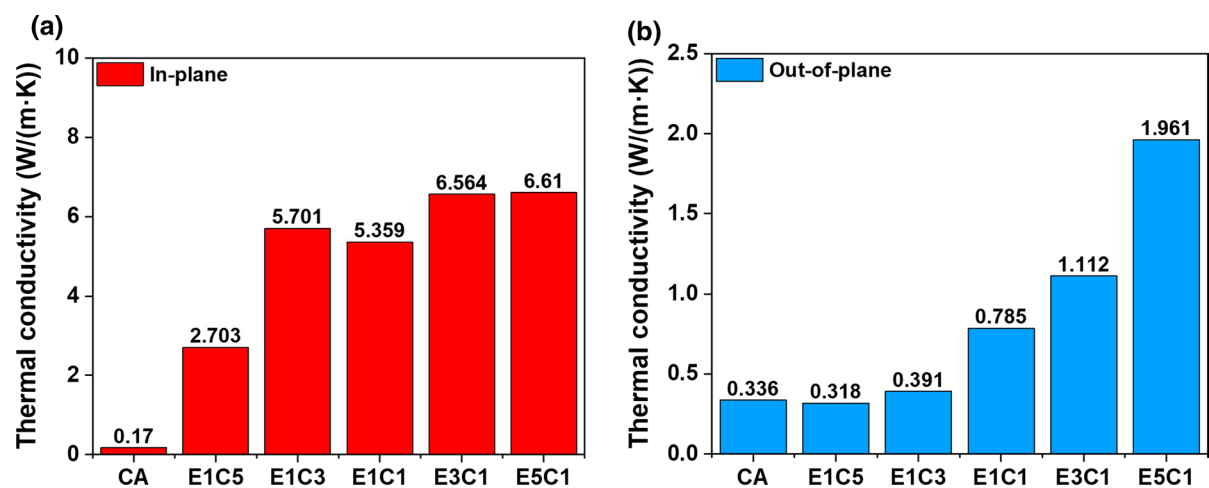


Fig. 5 (a) In-plane thermal conductivity  $K(\parallel)$  and (b) out-of-plane thermal conductivity  $K(\perp)$  of GNP/CA composite films

As shown in Fig. 6, E1C5 has a tensile strength of 27.17 MPa, higher than that of CA (25.77 MPa). With the increase of EG/CA ratio, the tensile strength of composite is increased accordingly, and obtains a peak value of 37.1 MPa at EG/CA ratio of 1:1, achieving a significant increase of 44%. This enhancement in tensile strength is due to the reason that the excellent compatibility between GNPs and CA facilitates the load transfer from CA to GNPs which has an ultra-high Young's modulus of 1 TPa and tensile strength of 130 GPa (Kabiri & Namazi. 2014; Lee et al. 2008; Malho et al. 2012; McAllister et al. 2007). However, further increasing EG/CA ratio up to 5:1 leads to the decline of tensile strength down to 13.77 MPa. The reason for this deterioration in tensile strength will be discussed in the following section.

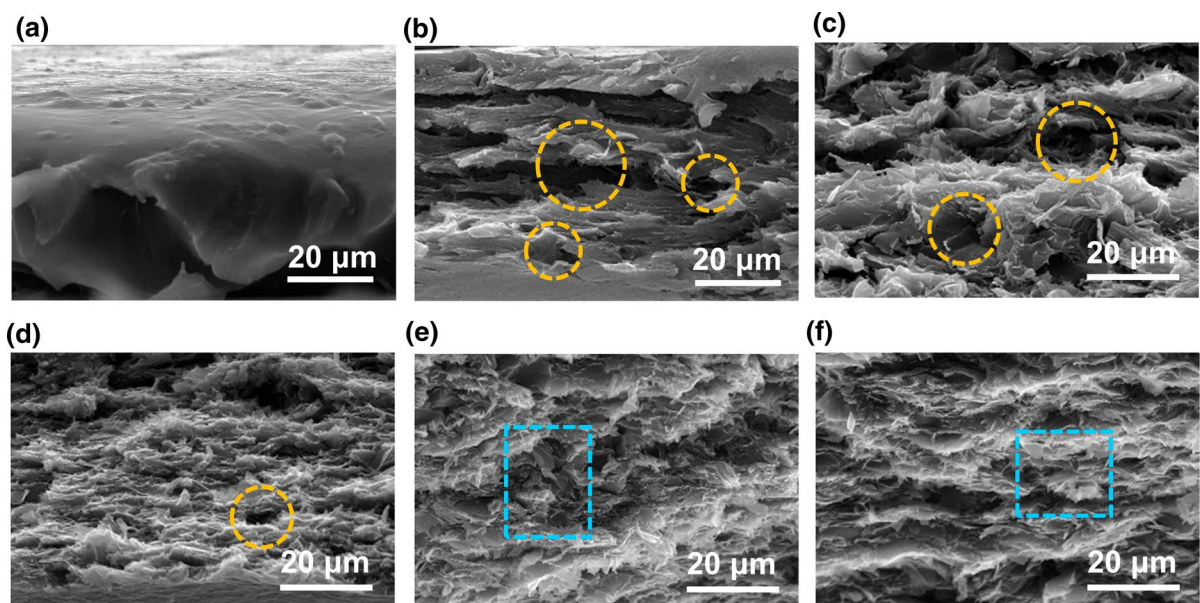
#### Morphology of GNP/CA composite films

Figure 7 shows the cross-section of GNP/CA composite films. Pure CA adopts a uniform structure (Fig. 7a) while GNP/CA composites have a rougher morphology. Moreover, layered-structure is observed in GNP/CA composites, which might originate from the self-assembly of GNPs during the solvent casting process. With the increase of the EG/CA ratio to 1/1,

the cross-section of the composite becomes denser, and the number and size of hole & pore is reduced (yellow circles in Fig. 7b, c, d). Together with the increase of GNP content (Fig. 3b), the composite thus has an increased tensile strength,  $K(\parallel)$ ,  $K(\perp)$  and improved antistatic property. However, as the EG/CA ratio further increases to 3/1 and 5/1, layered-structure gradually disappears and GNPs start to be randomly distributed due to the sharp increase of GNP content from 5.17% (for E1C1) to 22.81% (for E3C1) and further to 32.81% (for E5C1). Together with the increased defect on surfaces (Fig. S3), the as-prepared composites show decreased tensile strength, slightly changed  $K(\parallel)$  and surface resistivity but continuously increased  $K(\perp)$ .

#### Conclusions

In this work, we have produced GNP/CA composite films by the simple liquid exfoliation and solvent casting processes. Due to the spontaneous absorption of CA during liquid exfoliation, the GNPs with CA produced have an excellent dispersibility in DMF and much fewer structural defects compared to GNPs alone. Consequently, the as-prepared GNP/CA composite films show simultaneously and



**Fig. 7** SEM images of the cross-section of composite films. (a) pure CA, (b) E1C5, (c) E1C3, (d) E1C1, (e) E3C1 and (f) E5C1



significantly enhanced antistatic property, thermal conductivity and tensile strength, hence capable of rapid dissipation of static electricity and heat. Together with its biodegradability, promising overall performances and easy production etc., the GNP/CA composite film is promising to be commercialized for packaging.

**Author contributions** The manuscript was written through contributions of all authors. All authors have given approval to the final version of the manuscript.

**Funding** This work was financially supported by the National Natural Science Foundation of China (No. 52173067, 51803016, 11872132, U1837204, and 11672049), the Start-up Funding of Chongqing University (No. 0241001104454, 0903005203352, and 0241001104417), the Fund for Innovative Research Groups of Natural Science Foundation of Hebei Province (A2020202002), and the Science and Technology Project of Hebei Education Department (No. QN2021046).

**Data availability** The authors confirm that the data supporting the findings of this study are available within the article [and/or] its supplementary materials.

#### Declarations

**Conflict of interest** The authors declare no competing interests.

#### References

- Alqus R, Eichhorn S, Bryce R (2015) Molecular dynamics of cellulose amphiphilicity at the graphene–water interface. *Biomacromol* 16:1771–1783. <https://doi.org/10.1021/acs.biomac.5b00307>
- Araujo T, Bernardo G, Mendes A (2020) Cellulose-based carbon molecular sieve membranes for gas separation: a review. *Molecules* 25(15):3532. <https://doi.org/10.3390/molecules25153532>
- Balandin AA (2011) Thermal properties of graphene and nanostructured carbon materials. *Nat Mater* 10(8):569–581. <https://doi.org/10.1038/nmat3064>
- Balandin AA, Ghosh S, Bao W et al (2008) Superior thermal conductivity of single-layer graphene. *Nano Lett* 8(3):902–907. <https://doi.org/10.1021/nl0731872>
- Basu S, Hariharan KS, Kolake SM et al (2016) Coupled electrochemical thermal modelling of a novel Li-ion battery pack thermal management system. *Appl Energy* 181:1–13. <https://doi.org/10.1016/j.apenergy.2016.08.049>
- Biswas S, Drzal LT (2009) A novel approach to create a highly ordered monolayer film of graphene nanosheets at the liquid-liquid interface. *Nano Lett* 9(1):167–172. <https://doi.org/10.1021/nl802724f>
- Buchanan CM, Gardner RM, Komarek RJ (1993) Aerobic biodegradation of cellulose acetate. *J Appl Polym Sci* 47:1709–1719
- Claro PIC, Neto ARS, Bibbo ACC et al (2016) Biodegradable blends with potential use in packaging: a comparison of PLA/chitosan and PLA/cellulose acetate films. *J Polym Environ* 24(4):363–371. <https://doi.org/10.1007/s10924-016-0785-4>
- de Moraes AC, Andrade PF, de Faria AF et al (2015) Fabrication of transparent and ultraviolet shielding composite films based on graphene oxide and cellulose acetate. *Carbohydr Polym* 123:217–227. <https://doi.org/10.1016/j.carbpol.2015.01.034>
- Dong T, Yun X, Li M et al. (2015) Biodegradable high oxygen barrier membrane for chilled meat packaging. *J Appl Polym Sci* 132(16):n/a-n/a <https://doi.org/10.1002/app.41871>
- El-Din LAN, El-Gendi A, Ismail N et al (2015) Evaluation of cellulose acetate membrane with carbon nanotubes additives. *J Ind Eng Chem* 26:259–264. <https://doi.org/10.1016/j.jiec.2014.11.037>
- Elmaghraby NA, Omer AM, Kenawy E-R et al (2022) Electrospun composites nanofibers from cellulose acetate/carbon black as efficient adsorbents for heavy and light machine oil from aquatic environment. *J Iran Chem Soc* 19(7):3013–3027. <https://doi.org/10.1007/s13738-022-02510-1>
- Farivar F, Lay Yap P, Karunagaran RU et al (2021) Thermogravimetric analysis (TGA) of graphene materials: effect of particle size of graphene, graphene oxide and graphite on thermal parameters. *C* 7(2):41. <https://doi.org/10.3390/c7020041>
- Fei P, Liao L, Cheng B et al (2017) Quantitative analysis of cellulose acetate with a high degree of substitution by FTIR and its application. *Anal Methods* 9(43):6194–6201. <https://doi.org/10.1039/c7ay02165h>
- Gemili S, Yemenicioğlu A, Altunkaya SA (2009) Development of cellulose acetate based antimicrobial food packaging materials for controlled release of lysozyme. *J Food Eng* 90(4):453–462. <https://doi.org/10.1016/j.jfoodeng.2008.07.014>
- Groop E, Nowicki A, Calle C et al. (2003) Comparison of surface resistivity and triboelectric charge generation characteristics of materials. *Space Congress Proceedings*
- Han X, Gao J, Chen T et al (2019) Interfacial interaction and steric repulsion in polymer-assisted liquid exfoliation to produce high-quality graphene. *Chem Zvesti* 74(3):757–765. <https://doi.org/10.1007/s11696-019-00928-1>
- Ho Shin D, Han Yoon K, Hyeong Kwon O et al (2006) Surface resistivity and rheological behaviors of carboxylated multiwall carbon nanotube-filled PET composite film. *J Appl Polym Sci* 99(3):900–904. <https://doi.org/10.1002/app.21982>
- Iradukunda AC, Huitink DR, Luo F (2020) A review of advanced thermal management solutions and the implications for integration in high-voltage packages. *IEEE Trans Emerg Sel Topics Power Electron* 8(1):256–271. <https://doi.org/10.1109/JESTPE.2019.2953102>
- Jiang W, Nadeau G, Zaghbi K et al (2000) Thermal analysis of the oxidation of natural graphite — effect of particle size.

- Thermochim Acta 351(1):85–93. [https://doi.org/10.1016/S0040-6031\(00\)00416-0](https://doi.org/10.1016/S0040-6031(00)00416-0)
- Kabiri R, Namazi H (2014) Nanocrystalline cellulose acetate (NCCA)/graphene oxide (GO) nanocomposites with enhanced mechanical properties and barrier against water vapor. *Cellulose* 21(5):3527–3539. <https://doi.org/10.1007/s10570-014-0366-4>
- Kaiser A, Stark WJ, Grass RN (2017) Rapid production of a porous cellulose acetate membrane for water filtration using readily available chemicals. *J Chem Educ* 94(4):483–487. <https://doi.org/10.1021/acs.jchemed.6b00776>
- Konwarh R, Misra M, Mohanty AK et al (2013) Diameter-tuning of electrospun cellulose acetate fibers: a Box-Behnken design (BBD) study. *Carbohydr Polym* 92(2):1100–1106. <https://doi.org/10.1016/j.carbpol.2012.10.055>
- Lazarevic D, Aoustin E, Buclet N et al (2010) Plastic waste management in the context of a European recycling society: comparing results and uncertainties in a life cycle perspective. *Resour Conserv Recycl* 55(2):246–259. <https://doi.org/10.1016/j.resconrec.2010.09.014>
- Lee C, Wei X, Kysar JW et al (2008) Measurement of the elastic properties and intrinsic strength of monolayer graphene. *Science* 321(5887):385–388. <https://doi.org/10.1126/science.1157996>
- Lee MG, Lee S, Cho J et al (2020) Improving dispersion and mechanical properties of polypropylene/graphene nanoplatelet composites by mixed solvent-assisted melt blending. *Macromol Res* 28(12):1166–1173. <https://doi.org/10.1007/s13233-020-8144-7>
- Liu L, Shen Z, Liang S et al (2013) Graphene for reducing bubble defects and enhancing mechanical properties of graphene/cellulose acetate composite films. *J Mater Sci* 49(1):321–328. <https://doi.org/10.1007/s10853-013-7708-8>
- Malho JM, Laaksonen P, Walther A et al (2012) Facile method for stiff, tough, and strong nanocomposites by direct exfoliation of multilayered graphene into native nanocellulose matrix. *Biomacromol* 13(4):1093–1099. <https://doi.org/10.1021/bm2018189>
- Mangaraj S, Yadav A, Bal LM et al (2018) Application of biodegradable polymers in food packaging industry: a comprehensive review. *J Packag Technol Res* 3(1):77–96. <https://doi.org/10.1007/s41783-018-0049-y>
- McAllister MJ, Li J-L, Adamson DH et al (2007) Single sheet functionalized graphene by oxidation and thermal expansion of graphite. *Chem Mater* 19(18):4396–4404. <https://doi.org/10.1021/cm0630800>
- Morishita T, Matsushita M (2021) Ultra-highly electrically insulating carbon materials and their use for thermally conductive and electrically insulating polymer composites. *Carbon* 184:786–798. <https://doi.org/10.1016/j.carbon.2021.08.058>
- Muhmed SA, Nor NAM, Jaafar J et al (2020) Emerging chitosan and cellulose green materials for ion exchange membrane fuel cell: a review. *Energ Ecol Environ* 5(2):85–107. <https://doi.org/10.1007/s40974-019-00127-4>
- Naboka O, Yim C-H, Abu-Lebdeh Y (2016) Graphene/Na carboxymethyl cellulose composite for Li-ion batteries prepared by enhanced liquid exfoliation. *Mater Sci Eng B* 213:41–50. <https://doi.org/10.1016/j.mseb.2016.04.003>
- Nagarajan V, Mohanty AK, Misra M (2016) Perspective on polylactic acid (PLA) based sustainable materials for durable applications: focus on toughness and heat resistance. *ACS Sustain Chem Eng* 4(6):2899–2916. <https://doi.org/10.1021/acssuschemeng.6b00321>
- Novoselov KS, Fal'ko VI, Colombo L et al (2012) A roadmap for graphene. *Nature* 490(7419):192–200. <https://doi.org/10.1038/nature11458>
- Rajeswari A, Vismaiya S, Pius A (2017) Preparation, characterization of nano ZnO-blended cellulose acetate-polyurethane membrane for photocatalytic degradation of dyes from water. *Chem Eng J* 313:928–937. <https://doi.org/10.1016/j.cej.2016.10.124>
- Rajeswari A, Christy EJS, Swathi E et al (2020) Fabrication of improved cellulose acetate-based biodegradable films for food packaging applications. *Environ Chem Ecotoxicol* 2:107–114. <https://doi.org/10.1016/j.enceco.2020.07.003>
- Samantaray PK, Little A, Haddleton DM et al (2020) Poly(glycolic acid) (PGA): a versatile building block expanding high performance and sustainable bioplastic applications. *Green Chem* 22(13):4055–4081. <https://doi.org/10.1039/d0gc01394c>
- Seddiqi H, Oliaei E, Honarkar H et al (2021) Cellulose and its derivatives: towards biomedical applications. *Cellulose* 28(4):1893–1931. <https://doi.org/10.1007/s10570-020-03674-w>
- Shaikh S, Yaqoob M, Aggarwal P (2021) An overview of biodegradable packaging in food industry. *Curr Res Food Sci* 4:503–520. <https://doi.org/10.1016/j.crfcs.2021.07.005>
- Suthabanditpong W, Takai C, Razavi-Khosroshahi H et al (2019) Influence of CaCO<sub>3</sub> pore-forming agent on porosity and thermal conductivity of cellulose acetate materials prepared by non-solvent induced phase separation. *Adv Powder Technol* 30(1):207–213. <https://doi.org/10.1016/j.appt.2018.10.024>
- Taepaiboon P, Rungsardthong U, Supaphol P (2007) Vitamin-loaded electrospun cellulose acetate nanofiber mats as transdermal and dermal therapeutic agents of vitamin A acid and vitamin E. *Eur J Pharm Biopharm* 67(2):387–397. <https://doi.org/10.1016/j.ejpb.2007.03.018>
- Tan C, Dong Z, Li Y et al (2020) A high performance wearable strain sensor with advanced thermal management for motion monitoring. *Nat Commun* 11(1):3530. <https://doi.org/10.1038/s41467-020-17301-6>
- Tkalya EE, Ghislandi M, de With G et al (2012) The use of surfactants for dispersing carbon nanotubes and graphene to make conductive nanocomposites. *Curr Opin Colloid Interface Sci* 17(4):225–232. <https://doi.org/10.1016/j.cocis.2012.03.001>
- van Someren H, Beijersbergen van Henegouwen H, Los W et al (1974) Enzyme electrophoresis on cellulose acetate gel. II. Zymogram patterns in man-Chinese hamster somatic cell hybrids. *Humangenetik* 25(3):189–201. <https://doi.org/10.1007/bf00281426>
- Vu MC, Tran TS, Bae YH et al (2018) Self-assembly of carbon nanotubes and boron nitride via electrostatic interaction for epoxy composites of high thermal conductivity and electrical resistivity. *Macromol Res* 26(6):521–528. <https://doi.org/10.1007/s13233-018-6076-2>

- Wang Q, Wang Y, Meng Q et al (2017) Preparation of high antistatic HDPE/polyaniline encapsulated graphene nanoplatelet composites by solution blending. *RSC Adv* 7(5):2796–2803. <https://doi.org/10.1039/c6ra26458a>
- Wang Z, Wang D, Fang Y et al (2018) Preparation and properties of antistatic polyethylene film coated polypropylene non-woven fabrics. *Fibers Polymers* 19(5):934–940. <https://doi.org/10.1007/s12221-018-8048-8>
- Wondraczek H, Petzold-Welcke K, Fardim P et al (2013) Nanoparticles from conventional cellulose esters: evaluation of preparation methods. *Cellulose* 20(2):751–760. <https://doi.org/10.1007/s10570-013-9874-x>
- Wu F, Misra M, & Mohanty A K (2021) Challenges and new opportunities on barrier performance of biodegradable polymers for sustainable packaging. *Prog Polym Sci* 117:101395 <https://doi.org/10.1016/j.progpolymsci.2021.101395>
- Zhang K, Feldner A, Fischer S (2011) FT Raman spectroscopic investigation of cellulose acetate. *Cellulose* 18(4):995–1003. <https://doi.org/10.1007/s10570-011-9545-8>
- Zugenmaier P (2004) Characterization and physical properties of cellulose acetates. *Macromol Symp* 208(1):81–166. <https://doi.org/10.1002/masy.200450407>

**Publisher's Note** Springer Nature remains neutral with regard to jurisdictional claims in published maps and institutional affiliations.

Springer Nature or its licensor (e.g. a society or other partner) holds exclusive rights to this article under a publishing agreement with the author(s) or other rightsholder(s); author self-archiving of the accepted manuscript version of this article is solely governed by the terms of such publishing agreement and applicable law.